EVALUATING THE ACCURACY OF DAILY SATELLITE-BASED PRECIPITATION ESTIMATES (SPE) FOR RUNOFF ESTIMATION USING THE FLEX-TOPO-SD MODEL

Prasertthonggorn N.[1], Maekan E.[1], Kaprom C.[1,2,3], Kowsuvon N.[2,3], Ophaphabun C.[1], Kaewmee W.[2,3], Williams J.[1], and Sriwongsitanon N.*[1,2]

ABSTRACT

Rainfall data is essential for hydrological modeling and water resource management; however, ground-based observations are often sparse, particularly in remote regions. To address this limitation, satellite-based precipitation estimate (SPE) have emerged as viable alternatives, providing consistent spatial and temporal coverage where in-situ data is lacking. This study evaluated the performance of ten SPE products—categorized as satellite-only, satellite-gauge combined, and ensemble types—for daily runoff estimation in the Chi River Basin (CRB), located in Northeastern Thailand. The FLEX-TOPO-SD semi-distributed hydrological model was employed for this purpose.

The ten SPE products included five satellite-based datasets (CHIRP-V2, GPM IMERG-Early, GPM IMERG-Late, PERSIANN, and PERSIANN-CCS), four satellite-gauge products (CHIRPS-V2, CMORPH-BLD, GPM IMERG-Final, and PERSIANN-CDR), and one ensemble product (MSWEP V2). Their performance was assessed against a gridded gauged rainfall (GGR) dataset covering the period from 2001 to 2021. Model calibration was conducted from 2001 to 2015, and validation from 2016 to 2021, focusing on the downstream station E.20A and seven additional stations across the basin.

The results showed that satellite-gauge products generally aligned more closely with GGR than satellite-based products. Notably, CHIRP, a satellite-based dataset, also demonstrated strong performance. Among all products, MSWEP, GPM_FINAL, and CHIRPS yielded the most accurate rainfall estimates across daily, monthly, and annual scales.

Runoff simulations using the FLEX-TOPO-SD model revealed that MSWEP and GPM_FINAL produced outputs comparable to, and in some cases better than, those based on GGR, particularly during both calibration and validation periods. Across all stations, satellite-gauge products consistently outperformed satellite-only products. Conversely, the PERSIANN family—especially PERSIANN_CCS—exhibited significantly lower performance than GGR.

These findings highlight the potential of selected SPE products, particularly MSWEP, GPM_FINAL, and CHIRPS, as reliable alternatives to traditional gauge-based rainfall data in hydrological modeling for data-scarce regions. They also confirm the reliability and applicability of the FLEX-TOPO-SD model for regional-scale runoff estimation.

Keywords: Satellite-Based Precipitation Estimate; Runoff Estimation; FLEX-TOPO-SD Model; Chi River Basin; Thailand.

[1] Remote Sensing Research Centre for Water Resources Management (SENSWAT), Water Resources Engineering, Faculty of Engineering, Kasetsart University, Bangkok, Thailand

[2] Thai National Committee on Irrigation and Drainage (THAICID), Bangkok, Thailand

[3] Royal Irrigation Department (RID), Bangkok, Thailand

Correspondence: fengnns@ku.ac.th

1. INTRODUCTION

Rainfall is a key component of the hydrological cycle and is vital for runoff modeling, flood and drought forecasting, agricultural planning, and water resource management (Tapas et al., 2024; Nguyen et al., 2024; Nadeem et al., 2022; Quan et al., 2022; Ranjan et al., 2025). Accurate rainfall data is essential for informed decision-making. However, collecting field-based data requires substantial financial, technical, and human resources, making it particularly difficult in remote or mountainous areas (Skofronick-Jackson et al., 2017; Garova et al., 2025; Zamani et al., 2025). These challenges are even more pronounced in developing countries, where limited funding, difficult terrain, and inadequate infrastructure hinder the establishment of comprehensive meteorological networks (Hughes, 2006). As a result, many regions suffer from data gaps that compromise the accuracy of hydrological models and limit the effectiveness of water resource planning and disaster risk management.

Satellite-based precipitation estimate (SPE) products offer a practical alternative to rain gauge data, providing broad coverage and capturing rainfall variability (Wen et al., 2021; Lui et al., 2025; Nguyen et al., 2025). Early satellite-based (S) products, based on infrared and microwave data, offer quick access but are limited by biases (Kidd & Huffman, 2011; Dao et al., 2025). To enhance accuracy, satellite-gauge (SG) products combine satellite data with ground observations (Kaprom et al., 2025; Sriwongsitanon et al., 2023; Hussein et al., 2025). Additionally, MSWEP (Beck et al., 2017) is a global ensemble precipitation product that combines satellite, reanalysis, and gauge data using a weighted averaging approach. In this system, gauge weights are determined by station density, while satellite and reanalysis weights are based on their consistency with nearby gauge observations. Despite advancements, ground-based measurements remain essential for validating and correcting SPE data (Habib et al., 2014; Gumindoga et al., 2019). Bias correction of SPE products is often challenging due to limited ground data, variable satellite biases, and inaccessible terrain (Zhou et al., 2022). Consequently, rainfall-runoff models are commonly used to integrate satellite data with watershed features for streamflow simulation in data-scarce regions (Jahanshahi et al., 2024; Gautam et al., 2025; Muñoz et al., 2025).

Lumped rainfall-runoff models, such as SCS (Sharma & Singh, 1992), NAM (Gan et al., 1997; Ghosh et al., 2022), FLEXL (Fenicia et al., 2008; Sriwongsitanon et al., 2016), and FLEX-TOPO (Savenije, 2010; Gao et al., 2014, 2016), are commonly used for runoff estimation using areal rainfall data. However, they may lack precision in smaller catchments when applied to large areas. Semi-distributed models like URBS (Malone, 1999; Carroll, 2004; Mapiam & Sriwongsitanon, 2009; Sriwongsitanon, 2010), SWAT (Arnold et al., 2012; Gassman et al., 2014; Hlaing et al., 2024), FLEX-SD (Sriwongsitanon et al., 2023), and FLEX-TOPO-SD (Prasertthonggorn & Sriwongsitanon, 2022) provide more detailed and accurate assessments for smaller catchments.

This study aimed to assess the reliability of ten SPE products across three categories, satellite-based (S), satellite-gauge combined (SG), and ensemble products, as input data for runoff estimation using FLEX-TOPO-SD, a semi-distributed rainfall-runoff model. The evaluation was conducted in the Chi River Basin (CRB) located in northeastern Thailand. Runoff estimations derived from the ten SPE products were assessed at eight stations within the basin and compared against results obtained using gridded gauged rainfall (GGR), which was generated from gauge data collected within and around the CRB.

2. STUDY AREA

Runoff estimation using the FLEX-TOPO-SD model was applied to the Chi River Basin (CRB) in northeastern Thailand. The basin covers an area of approximately 49,132 km² and was divided into 98 sub-catchments to assess runoff at the outlet of each sub-catchment (see **Figure 1**). The Chi River, which is the main river flowing through the basin, extends for about 830 km. The basin's topography varies from the highlands of the Phetchabun Mountains, reaching up to 1,250 meters, to the low-lying floodplains at around 150 meters. Most of the terrain is relatively flat, with slopes of less than 10%.

The CRB lies within the tropical monsoon zone and is influenced by both the southwest and northeast monsoons. The region experiences a semi-arid climate, with average annual rainfall ranging from 1,170 to 1,279 mm. Most of the rainfall, approximately 89%, occurs during the rainy season from May to October, while the remaining 11% falls during the dry season from November to April.

Two large-scale reservoirs are located within the basin: the Ubol Ratana Reservoir, with an active storage capacity of 2,431 million cubic meters, and the Lam Pao Reservoir, with a capacity of 1,430 million cubic meters. The dominant land use types in the basin are field crops and rice paddies, which account for 32.39% and 29.29% of the area, respectively. In contrast, forested areas make up only about 17% of the basin (Land Development Department of Thailand, 2021).

For the semi-distributed model, the CRB is divided into 98 sub-catchments, as shown in **Figure 1**.

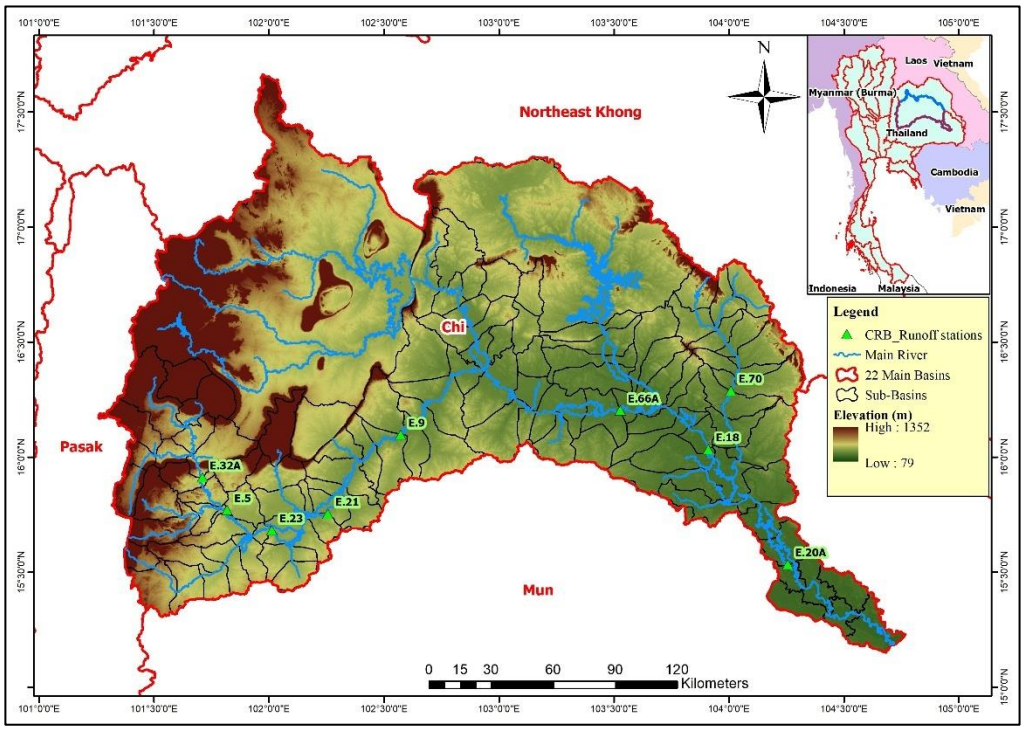

Figure 1. Topography of the Chi River Basin.

3. METHODS

3.1 Data collection

(3.1.1) Rainfall Data

(i) Gridded Gauged Rainfall (GGR) Data

Daily GGR data with a spatial resolution of 1 km for the period 2001–2021 were developed for the entirety of Thailand. These data were compiled using daily rainfall records from 1,150 stations operated by the Thailand Meteorological Department (TMD), 582 stations from the Royal Irrigation Department (RID), and 47 stations from other organizations. To ensure data accuracy and reliability, this study applied a 14-step quality control procedure proposed by Hamada et al. (2011), which includes metadata checks, station-level verification, and cross-station consistency assessments.

(ii) Satellite-based precipitation estimate (SPE) products

This study includes ten precipitation products, comprising individual satellite-derived datasets and ensemble products. The individual satellite-derived products are divided into two categories: satellite-based precipitation products (S) and satellite-gauge precipitation products (SG).

A total of nine individual satellite-derived products were selected for analysis. Within the S category, five products were included: CHIRP-V2, GPM IMERG-Early-V6, GPM IMERG-Late-V6, PERSIANN, and PERSIANN-CCS. The SG category consists of four products: CMORPH-BLD-V1.0, CHIRPS-V2.0, GPM IMERG-Final-V6, and PERSIANN-CDR. An overview of the SPE products used in this study is provided in **Table 1**.

Additionally, the study considers ensemble products, which are created by combining multiple data sources, including gauged rainfall and reanalysis data. One of the most widely recognized ensemble products is the Multi-Source Weighted-Ensemble Precipitation (MSWEP) Version 2, developed by Beck et al. (2019). MSWEP V2 is notable for being the first fully global precipitation dataset, providing data from 1979 to the present. It is available for download at http://www.gloh2o.org. Descriptions of the ensemble SPE products are presented in **Table 2**.

Table 1. Overview of SPE Products used in this study

	Integrated Multi-satellites for GPM (IMERG)	Climate Hazards Group Infrared Precipitation with Stations (CHIRPS)	Climate Prediction Centre MORPHing method (CMORPH)	Precipitation Estimation from Remotely Sensed Information using Artificial Neural Networks (PERSIANN)
Satellite-based (S) product	- GPM IMERG-Early - GPM IMERG-Late	- CHIRP	-	- PERSIANN - PERSIANN-CCS
Satellite-gauge (SG) product	- GPM IMERG Final (GPCC gauge analysis)	- CHIRPS (Several other stations sources)	- CMORPH-BLD (CPC unified daily gauge analysis)	- PERSIANN-CDR (GPCP monthly precipitation)
References	Huffman et al., 2007; 2010	Funk et al., 2015	Joyce et al., 2004	Hsu et al., 1997, Sorooshian et al., 2000
Available at	https://gpm1.gesdisc.eosdis.nasa.gov/data/GPM_L3_	http://chg.geog.ucsb.edu/data/chirps_	ftp://ftp.cpc.ncep.noaa.gov/precip/CMORPH_V1.0_	https://chrsdata.eng.uci.edu/

Table 2. Descriptions of the satellite precipitation estimate (SPE) products utilized in this study

Products	Temporal Resolution	Latency	Available Period	Spatial Resolution	Spatial Coverage
Satellite-based precipitation (S) product					
1. CHIRP-V2.0*	1 day	2 days	1981 – Present	0.05°	50°S–50°N
2. GPM IMERG-Early-V6*	30 mins	6 hours	2000 – Present	0.10°	90°S–90°N
3. GPM IMERG-Late-V6*	30 mins	18 hours	2000 – Present	0.10°	90°S–90°N
4. PERSIANN*	1 hour	2 days	2000 – Present	0.25°	60°S–60°N
5. PERSIANN-CCS*	1 hour	1 hours	2003 – Present	0.04°	60°S–60°N
Satellite-gauge precipitation (SG) product					
1. CMORPH-BLD-V1.0	1 day	2 months	1998 – Present	0.25°	60°S–60°N
2. CHIRPS-V2.0	1 day	3 weeks	1981 – Present	0.05°	50°S–50°N
3. GPM IMERG-Final-V6	30 mins	3.5 months	2000 – Present	0.10°	90°S–90°N
4. PERSIANN-CDR	1 day	3 months	1983 – Present	0.25°	60°S–60°N
Ensemble products					
1. MSWEP V2	1 day	3 hours	1979 – Present	0.10°	90°S–90°N

Note: * Indicates S product

(3.1.2) Runoff Data

A total of eight runoff stations in the CRB were selected for runoff estimation using the FLEX-TOPO-SD model. These stations, operated by the Royal Irrigation Department (RID), include E.32A, E.5, E.23, E.21, E.9, E.66A, E.18, and E.20A.

Table 3 presents the catchment and hydrological characteristics of these gauging stations, along with land use data provided by the Land Development Department (LDD) for the period 2019–2021. The table also includes annual average rainfall and runoff data for each station, covering the period from 2001 to 2021. The average runoff coefficients range from approximately 14% at stations E.9 and E.66A to 26% at station E.32A.

Table 3. Catchment and hydrological characteristics of 8 gauging stations in the CRB

Runoff Station	E.32A	E.5	E.23	E.21	E.9	E.66A	E.18	E.20A
Area (km^2)	2,877	4,207	6,771	8,806	10,918	31,758	41,278	47,721
Average Rainfall (mm/yr)	1,153	1,141	1,095	1,094	1,097	1,139	1,153	1,204
Runoff (mm/yr)	298	263	164	183	155	165	179	202
Average Runoff Coefficient (%)	26	23	15	17	14	14	16	17

(3.1.3) Potential Evapotranspiration (PET) Data

GLEAM (Global Land Evaporation Amsterdam Model) V4.2a (Miralles et al., 2025) is a satellite-based evapotranspiration dataset that provides global estimates of potential evapotranspiration (PET) and was selected as input for this study's hydrological modelling. The dataset is available at a daily temporal resolution from 1980 to the present, with an approximate latency of one year. For this study, only data from 2001 to 2021 were used to align with other available observational datasets.

GLEAM V4.2a estimates potential evapotranspiration (PET) using the Penman equation based on surface net radiation (Rn), near-surface air temperature (Ta), wind speed (u), leaf area index (LAI), and vapor pressure deficit (VPD).

It integrates reanalysis radiation and air temperature data, as well as precipitation and vegetation optical depth derived from various sources. With its physically based approach and consistent spatiotemporal coverage, GLEAM is well-suited for hydrological and drought studies. The dataset is available at ~10 km resolution and accessible via http://www.gleam.eu.

(3.1.4) Digital Elevation Model (DEM)

The Digital Elevation Model (DEM) covering the CRB, obtained from the Shuttle Radar Topography Mission (SRTM) and provided by the U.S. Geological Survey (USGS), was used in this study. It has a spatial resolution of 30 meters (Mukul et al., 2015). The DEM was used in the FLEX-TOPO-SD model to classify landscapes based on terrain characteristics.

3.2 Evaluation of SPE products compared to GGR Data

The accuracy of the SPE products was evaluated by comparing them with GGR data across the CRB and its 98 sub-catchments. The comparison covered the period from 2001 to 2021 and was conducted at daily, monthly, and annual timescales. Three statistical indicators were used to assess performance: the Kling-Gupta Efficiency (KGE), the coefficient of determination (R^2), and the relative root mean square error (Rel. RMSE).

3.3 Model calibration using FLEX-TOPO-SD

In this study, the FLEX-TOPO-SD model, a semi-distributed version of the lumped FLEX-TOPO model, is used to simulate rainfall-runoff processes. Originally developed by Gao et al. (2014) from the FLEXL model, FLEX-TOPO accounts for landscape-driven hydrological differences by classifying terrain into three types: Hillslope, Terrace, and Wetland. This classification is based on physical features such as the height above the nearest drainage (HAND) (Rennó et al., 2008) and land surface slope.

The FLEX-TOPO model classifies landscapes into three types based on HAND values and slope: Wetlands (HAND < 5 m), Terraces (HAND ≥ 5 m and slope < 0.1), and Hillslopes (HAND > 5 m and slope ≥ 0.1). Each type exhibits distinct runoff processes, as shown in **Figure 2**. The corresponding water balance and constitutive equations are summarized in **Table 4**.

The FLEX-TOPO model was further developed into FLEX-TOPO-SD, a semi-distributed hydrological model based on the framework proposed by Sriwongsitanon et al. (2023). In this approach, the catchment is divided into sub-catchments to estimate discharge individually. Excess rainfall is calculated for each sub-catchment and routed to its outlet using time lag parameters, TlagF and TlagS (in hours), which are determined using **Eq. (52)** and (**53)**.

$$T_{lagF-sub} = T_{lagF}\sqrt{A_{sub}/A} \tag{52}$$

$$T_{lagS-sub} = T_{lagS}\sqrt{A_{sub}/A} \tag{53}$$

Where, "A" represents the individual watershed areas, "TlagF" refers to the time delay parameter for the fast-responding reservoir, and "TlagS" represents the time delay parameter for groundwater.

The downstream volume of the sub-catchment ($S_{chnl\text{-}sub}$) flows from the upstream inlet to the downstream outlet using the Muskingum method before joining the flow at the downstream station's gauge point, as described by **Eq. (54)** and (**55)**.

$$S_{schnl-sub} = \propto_{sub} (XQ_{up} + (1-x)Q_{down}) \quad (54)$$

$$\propto_{sub} = \propto L_{sub} \quad (55)$$

Where "Q_{up}" and "Q_{down}" represent the upstream and downstream discharge, respectively. α is the time delay parameter, "X" is the weighting factor, and "L" is the distance from upstream inlet to downstream outlet. The time delay parameter for each sub-catchment (K_{sub}) is the product of K and the river channel length (L).

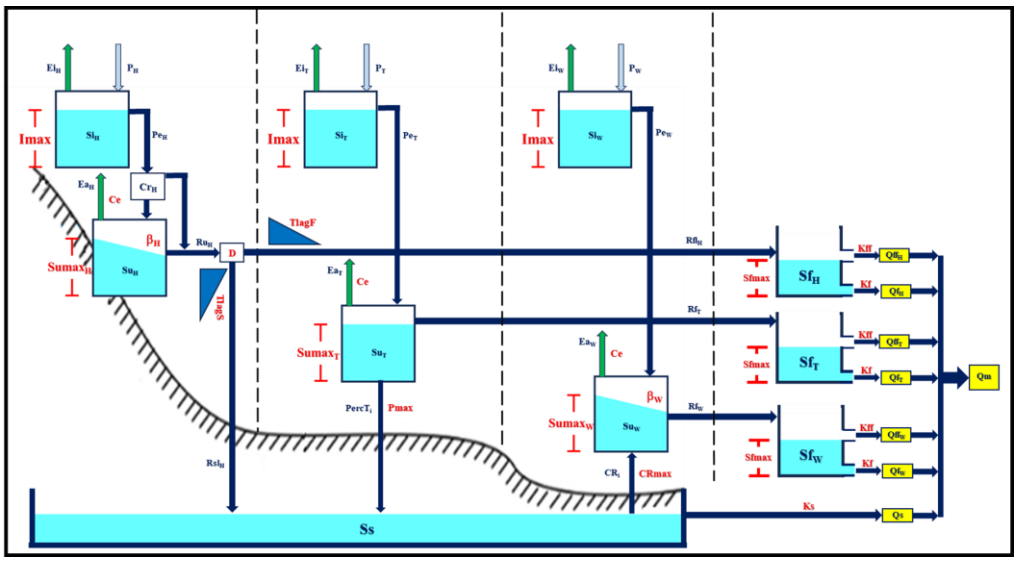

Figure 2. Model structure of FLEX-TOPO model.

The FLEX-TOPO-SD model was calibrated for the period 2001–2015 (~70%) and validated for 2016–2021 (~30%) in the CRB. Calibration was performed at station E.20A, while validation occurred at seven upstream stations. The model's performance was assessed at the calibration stations and validated against upstream stations using daily runoff estimates from the GGR dataset and ten SPE products, enabling a thorough evaluation of each SPE's accuracy in runoff estimation. Model optimization was performed using a multi-objective approach based on three criteria: KGE_E, KGE_L, and KGE_F.

Table 4. Water balance and constitutive equations for FLEX-TOPO

No.	Reservoir	Constitutive equations	Equation	Water balance Equation	Equation
1	Snow (Hillslope, Terrace, Wetland)	$M_i = \begin{cases} F_{DD}(T_i - Tt); T_i > Tt \\ 0 \quad ; T_i \le Tt \end{cases}$	(1)	$\frac{dSw_i}{dt} = Ps_i - M_i$	(2)
2	Interception (Hillslope, Terrace, Wetland)	$Ei_i = \begin{cases} \min((Si_{i-1} + P_i), Ep_i) & ; Si_i > 0 \\ 0 & ; Si_i = 0 \end{cases}$	(3)	$\frac{dSi_i}{dt} = Pi_i - Ei_i - Ptf_i$	(5)
		$Ptf_i = \begin{cases} 0 & ; Si_i < Imax \\ Pi_i + Si_{i-1} - Imax & ; Si_i \ge Imax \end{cases}$	(4)		
3	Unstuated soil	$Pe_i = Ptf_i + M_i$	(6)		
	Hillslope	$Cr_{H(i)} = 1 - \left(1 - \frac{Su_{H(i-1)}}{SumaxH}\right)^{\beta_H}$	(7)	$\frac{dSu_{H(i)}}{dt} = Pe_i(1 - Cr_{H(i)}) - Ea_{H(i)}$	(11)
		$Su_{H(i)} = Su_{H(i-1)} + Pe_i(1 - Cr_{H(i)})$	(8)		
		$Ru_{H(i)} = \begin{cases} Pe_i\, Cr_{H(i)} + (Su_{H(i)} - SumaxH) & ; Su_{H(i)} \ge SumaxH \\ Pe_i\, Cr_{H(i)} & ; Su_{H(i)} < \text{SumaxH} \end{cases}$	(9)		
		$Ea_{H(i)} = \min(Su_{H(i)}, (Ep_i - Ei_i), (Ep_i - Ei_i)\frac{Su_{H(i)}}{Ce * SumaxH})$	(10)		
	Terrace	$Su_{T(i)} = Su_{T(i-1)} + Pe_i$	(12)	$\frac{dSu_{T(i)}}{dt} = Pe_i(1 - Cr_{T(i)}) - Ea_{T(i)} - PercT_i$	(17)
		$Ru_{T(i)} = \begin{cases} Su_{T(i)} - SumaxT & ; Su_{T(i)} \ge SumaxT \\ 0 & ; Su_{T(i)} < \text{SumaxT} \end{cases}$	(13)		
		$Su_{T(i)} = \begin{cases} SumaxT & ; Su_{T(i)} \ge SumaxT \\ Su_{T(i)} & ; Su_{T(i)} < \text{SumaxT} \end{cases}$	(14)		
		$Ea_{T(i)} = \min(Su_{T(i)}, (Ep_i - Ei_i), (Ep_i - Ei_i)\frac{Su_{T(i)}}{Ce * SumaxT})$	(15)		
		$PercT_i = \min((Su_{T(i)} - Ea_{T(i)}), Pmax)$	(16)		
	Wetland	$Cr_{W(i)} = 1 - \left(1 - \frac{Su_{W(i-1)}}{SumaxW}\right)^{\beta_W}$	(18)	$\frac{dSu_i}{dt} = Pe_i - Ea_{W(i)} + CR_i$	(23)
		$Su_{W(i)} = Su_{W(i-1)} + Pe_i(1 - Cr_{W(i)})$	(19)		
		$Ru_{W(i)} = \begin{cases} Pe_i\, Cr_{W(i)} + (Su_{W(i)} - SumaxW) & ; Su_{W(i)} \ge SumaxW \\ Pe_i\, Cr_{W(i)} & ; Su_{W(i)} < \text{SumaxW} \end{cases}$	(20)		
		$Ea_{W(i)} = \min(Su_{W(i)}, (Ep_i - Ei_i), (Ep_i - Ei_i)\frac{Su_{W(i)}}{Ce * SumaxW})$	(21)		
		$CR_i = \min(Ss_{1(i)} + CRmax)$	(22)		
4	Fast response	$c_{lagF}(j) = \frac{j}{\sum_{u=1}^{T_{lagF}} u}$	(24)		
	Hillslope	$Rf_{H(i)} = Ru_{H(i)}D$	(25)	$\frac{dSf_{H(i)}}{dt} = Rfl_{H(i)} - Qff_{H(i)} - Qf_{H(i)}$	(30)
		$Rfl_{H(i)} = \sum_{j=1}^{T_{lagF}} C_{lagF}(j) \cdot Rf_{H(i-j-1)}$	(26)		
		$Sf_{H(i)} = Sf_{H(i-1)} + Rfl_{H(i)}$	(27)		
		$Qff_{H(i)} = \frac{\max(0, Sf_{H(i)} - Sfmax)}{Kff_H}$	(28)		
		$Qf_{H(i)} = \frac{Sf_{H(i)}}{Kf_H}$	(29)		
	Terrace	$Rf_{T(i)} = Ru_{T(i)}$	(31)	$\frac{dSf_{T(i)}}{dt} = Rfl_{T(i)} - Qff_{T(i)} - Qf_{T(i)}$	(36)
		$Rfl_{T(i)} = \sum_{j=1}^{T_{lagF}} C_{lagF}(j) \cdot Rf_{T(i-j-1)}$	(32)		
		$Sf_{T(i)} = Sf_{T(i-1)} + Rfl_{T(i)}$	(33)		
		$Qff_{T(i)} = \frac{\max(0, Sf_{T(i)} - Sfmax)}{Kff_T}$	(34)		
		$Qf_{T(i)} = \frac{Sf_{T(i)}}{Kf_T}$	(35)		
	Wetland	$Rf_{W(i)} = Ru_{W(i)}$	(37)	$\frac{dSf_{W(i)}}{dt} = Rfl_{W(i)} - Qff_{W(i)} - Qf_{W(i)}$	(42)
		$Rfl_{W(i)} = \sum_{j=1}^{T_{lagF}} C_{lagF}(j) \cdot Rf_{W(i-j-1)}$	(38)		
		$Sf_{W(i)} = Sf_{W(i-1)} + Rfl_{W(i)}$	(39)		
		$Qff_{W(i)} = \frac{\max(0, Sf_{W(i)} - Sfmax)}{Kff_W}$	(40)		
		$Qf_{W(i)} = \frac{Sf_{W(i)}}{Kf_W}$	(41)		
5	Slow response	$c_{lagS}(j) = \frac{j}{\sum_{u=1}^{T_{lagS}} u}$	(43)		
		$Rs_{(i)} = Ru_{H(i)}(1 - D)$	(44)		
		$Rsl_{(i)} = \sum_{j=1}^{T_{lagS}} C_{lagS}(j) \cdot Rs_{(i-j-1)}$	(46)	$\frac{dSs_{(i)}}{dt} = Rsl_{(i)} - Qs_{(i)}$	(50)
		$Ss_{1(i)} = Ss_{2(i-1)} + Rsl_{(i)} + PercT_i$	(47)		
		$Ss_{2(i)} = Ss_{1(i)} - CR_i$	(48)		
		$Qs_{(i)} = \frac{Ss_{2(i)}}{Ks}$	(49)		
		$\boldsymbol{Qm_{(i)} = (Qff_{H(i)} + Qf_{H(i)}) * propH + (Qff_{T(i)} + Qf_{T(i)}) * propT + (Qff_{W(i)} + Qf_{W(i)}) * propW + Qs_{(i)}}$	(51)		

4. RESULTS AND DISCUSSION

4.1 Accuracy of SPE Products Compared to GGR Data

Figure 3 compares annual and average rainfall in the CRB from 2001 to 2021, using data from GGR and ten SPE products. **Figure 3(a)** highlights noticeable differences in annual rainfall over the 21-year period between the SPE products and GGR. Although rainfall estimates from the SPE products vary significantly, the SG products show patterns more consistent with GGR than the S products, except for CHIRP*, which also closely matches GGR.

Figure 3(b) shows that the average monthly rainfall estimated by the SPE products is generally higher than that of GGR. As shown in **Figure 3(c)**, the five products with annual rainfall estimates closest to GGR are MSWEP, CHIRP*, CMORPH_BLD, CHIRPS, and GPM_FINAL, with differences of 0.2%, 1.6%, 8.1%, 14.4%, and 15.8%, respectively. Notably, although CHIRP* is an S product, it performs best during both wet and dry seasons, with deviations of 2.2% and -2.4%, respectively, compared to GGR.

Table 5 summarizes statistical indicators - including KGE, R^2, and relative RMSE -used to evaluate the accuracy of daily, monthly, and annual rainfall estimates from the ten SPE products relative to GGR in the CRB. The table also ranks the products by order of accuracy based on these indicators across different temporal scales. The results indicate that MSWEP consistently ranks first in accuracy across all time scales, followed by GPM_FINAL, CMORPH_BLD, CHIRPS, CHIRP*, GPM_LATE*, and GPM_EARLY*. In contrast, the three products from the PERSIANN family rank lowest in performance.

Figure 4 presents scatter plots comparing average annual rainfall (2001–2021) from GGR and ten SPE products across 98 sub-catchments. It also includes performance metrics—KGE, R^2, and relative RMSE—derived from these comparisons. The results indicate that CHIRP* provides the closest match to the GGR dataset in terms of average annual rainfall across the 98 sub-catchments. This is followed by MSWEP, CHIRPS, GPM_FINAL, CMORPH_BLD, GPM_EARLY*, and GPM_LATE*. In contrast, the PERSIANN family ranks lowest in performance.

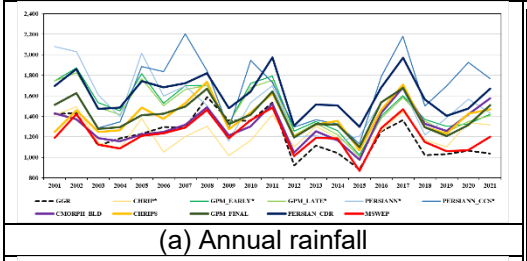

(a) Annual rainfall

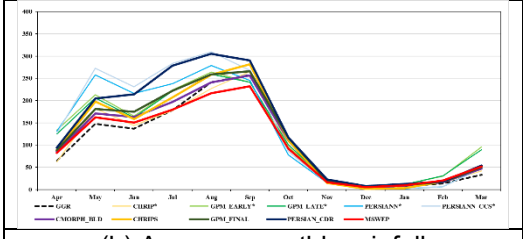

(b) Average monthly rainfall

Products	Rainfall (mm)					
	Wet Season (May - Oct)		Dry Season (Nov - Apr)		Annual	
Gridded Gauged Rainfall (GGR)						
1. GGR	1,073.3		142.8		1,216.1	
Satellite-based precipitation (S) product						
1. CHIRP*	1,096.5	(2.2%)	139.4	(-2.4%)	1,235.9	(1.6%)
2. GPM_EARLY*	1,202.2	(12.0%)	297.7	(108.4%)	1,499.8	(23.3%)
3. GPM_LATE*	1,190.8	(10.9%)	283.6	(98.6%)	1,474.4	(21.2%)
4. PERSIANN*	1,313.5	(22.4%)	205.7	(44.0%)	1,519.2	(24.9%)
5. PERSIANN_CCS*	1,450.5	(35.1%)	199.7	(39.8%)	1,650.3	(35.7%)
Satellite-gauge precipitation (SG) product						
1. CMORPH_BLD	1,136.5	(5.9%)	178.0	(24.6%)	1,314.4	(8.1%)
2. CHIRPS	1,212.6	(13.0%)	178.7	(25.1%)	1,391.3	(14.4%)
3. GPM_FINAL	1,218.6	(13.5%)	189.1	(32.4%)	1,407.7	(15.8%)
4. PERSIANN_CDR	1,410.0	(31.4%)	207.4	(45.2%)	1,617.4	(33.0%)
Ensemble products						
1. MSWEP	1,038.1	(-3.3%)	180.9	(26.7%)	1,219.0	(0.2%)

(c) Average annual and seasonal rainfall

Figure 3. Comparison of annual and average monthly rainfall (2001-2021) in the CRB using data from GGR and ten SPE products

Table 5. Statistical indicators of the accuracy of daily, monthly, and annual rainfall estimates from ten SPE products compared with GGR in the CRB

SPE products		CHRIP*	GPM_EARLY*	GPM_LATE*	PERSIANN*	PERSIANN_CCS*	CMORPH_BLD	CHRIPS	GPM_FINAL	PERSIAN_CDR	MSWEP
CRB											
KGE	Daily	0.70 (3)	0.50 (6)	0.50 (7)	0.33 (9)	0.25 (10)	0.72 (2)	0.66 (4)	0.61 (5)	0.48 (8)	0.85 (1)
	Monthly	0.92 (1)	0.74 (7)	0.77 (6)	0.63 (8)	0.48 (10)	0.91 (2)	0.83 (4)	0.82 (5)	0.59 (9)	0.90 (3)
	Annual	0.41 (8)	0.67 (4)	0.70 (3)	0.35 (9)	0.13 (10)	0.55 (7)	0.63 (5)	0.72 (2)	0.62 (6)	0.76 (1)
R^2	Daily	0.50 (7)	0.56 (6)	0.60 (4)	0.38 (10)	0.40 (9)	0.72 (2)	0.57 (5)	0.68 (3)	0.49 (8)	0.73 (1)
	Monthly	0.87 (6)	0.83 (8)	0.85 (7)	0.74 (10)	0.75 (9)	0.92 (4)	0.93 (3)	0.94 (1)	0.91 (5)	0.93 (2)
	Annual	0.23 (10)	0.66 (4)	0.69 (3)	0.34 (7)	0.27 (9)	0.33 (8)	0.47 (6)	0.70 (2)	0.66 (5)	0.74 (1)
rel. RMSE (%)	Daily	117% (3)	144% (7)	141% (6)	187% (9)	193% (10)	101% (2)	124% (5)	119% (4)	146% (8)	85% (1)
	Monthly	35% (5)	49% (7)	45% (6)	66% (9)	79% (10)	29% (2)	33% (4)	30% (3)	52% (8)	27% (1)
	Annual	19% (2)	34% (7)	31% (6)	41% (8)	55% (10)	21% (3)	25% (5)	24% (4)	45% (9)	11% (1)
Average (Rank)	Daily	**4.3 (4)**	**6.3 (7)**	**5.7 (6)**	**9.3 (9)**	**9.7 (10)**	**2.0 (2)**	**4.7 (5)**	**4.0 (3)**	**8.0 (8)**	**1.0 (1)**
	Monthly	**4.0 (5)**	**7.3 (7)**	**6.3 (6)**	**9.0 (9)**	**9.7 (10)**	**2.7 (2)**	**3.7 (4)**	**3.0 (3)**	**7.3 (7)**	**2.0 (1)**
	Annual	**6.7 (7)**	**5.0 (4)**	**4.0 (3)**	**8.0 (9)**	**9.7 (10)**	**6.0 (6)**	**5.3 (5)**	**2.7 (2)**	**6.7 (7)**	**1.0 (1)**
	Average	**5.0 (5)**	**6.2 (7)**	**5.3 (6)**	**8.8 (9)**	**9.7 (10)**	**3.6 (3)**	**4.6 (4)**	**3.2 (2)**	**7.3 (8)**	**1.3 (1)**

Note: The number in parentheses denotes the order of accuracy

4.2 Model performance in runoff estimation using GGR and ten SPE products

Table 6 presents statistical metrics for the calibrated station E.20A during the calibration period (2001–2015) and the validation period (2016–2021), using GGR and ten SPE products as input data for runoff estimation with the FLEX-TOPO-SD model. Model performance was assessed using three multi-objective criteria: KGE_E, KGE_L, and KGE_F. In addition, NSE was used as an independent performance indicator.

During the calibration period, MSWEP and GPM_FINAL performed best for runoff estimation at station E.20A, both achieving an NSE of 0.78. These were followed by GPM_EARLY* (0.75), CMORPH_BLD (0.71), CHIRPS (0.71), GGR (0.69), CHIRP* (0.66), and GPM_LATE* (0.63). The PERSIANN family ranked lowest, with PERSIANN_CCS* yielding a negative NSE. On average, the SG group achieved an NSE of 0.69, while the S group performed significantly worse, with an average NSE of 0.49.

In the validation period, MSWEP maintained the strongest performance with the highest NSE value of 0.86. GGR followed closely with an NSE of 0.83, while GPM_FINAL and GPM_LATE* recorded values of 0.79. CHIRPS reached 0.76, CHIRP* achieved 0.72, and GPM_EARLY* posted 0.71. In contrast, PERSIANN_CCS* once again showed the poorest performance, yielding a negative NSE. On average, the SG group recorded an NSE of 0.66, clearly outperforming the S group, which averaged a significantly lower NSE of 0.50.

Table 7 summarizes the average statistical metrics across eight stations for both the calibration and validation periods. During calibration, GPM_FINAL emerged as the top-performing product, yielding an NSE of 0.80. It was followed closely by GGR with 0.78, MSWEP with 0.77, and CHIRPS with 0.74. Other products, including GPM_EARLY*, CMORPH_BLD, GPM_LATE*, and CHIRP*, produced NSE values of 0.69, 0.68, 0.66, and 0.63, respectively. In contrast, PERSIANN_CCS delivered the weakest performance, with a negative NSE. Overall, the SG group demonstrated a higher average NSE of 0.70, in contrast to the S group, which showed a considerably lower average of 0.46.

In the validation period, MSWEP recorded the highest NSE value of 0.82, confirming its strong performance. This was followed by GGR with 0.78, GPM_FINAL with 0.73, and CHIRPS with 0.68. Moderate performance was observed for PERSIANN* (0.63), GPM_EARLY* (0.61), GPM_LATE* (0.54), and CMORPH_BLD (0.47). In contrast, PERSIANN_CCS* continued to perform poorly, showing a negative NSE. On average, the SG group achieved an NSE of 0.55, while the S group exhibited a significantly lower mean value of 0.12.

Runoff estimation using the FLEX-TOPO-SD model with GGR and ten SPE products was evaluated at station E.20A and across eight stations. MSWEP, GPM_FINAL, and GGR showed strong performance, with GGR consistently ranking among the top three. SG products outperformed S products in both calibration and validation, with higher average NSE values. PERSIANN_CCS* performed the worst.

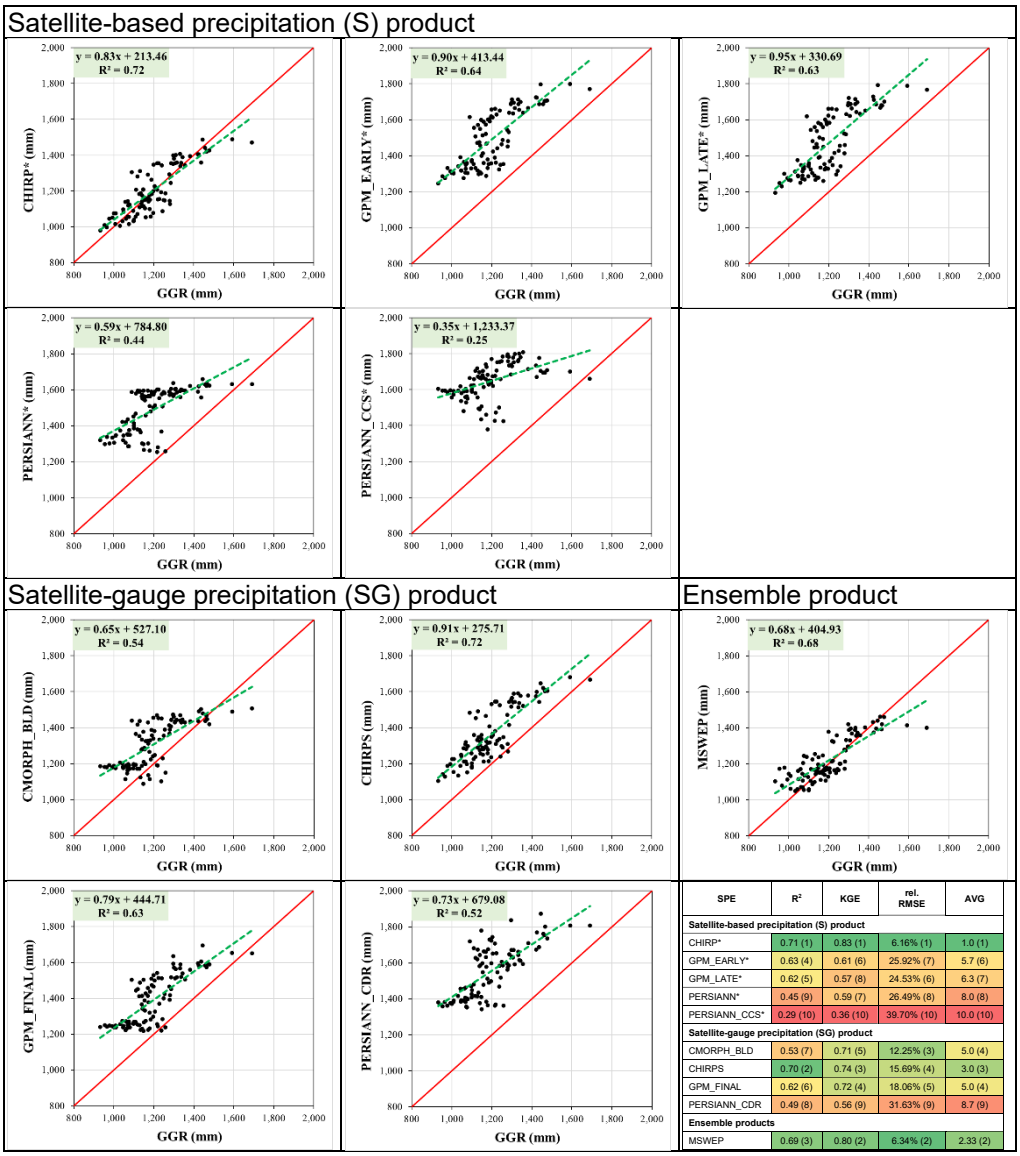

SPE	R^2	KGE	rel. RMSE	AVG
Satellite-based precipitation (S) product				
CHIRP*	0.71 (1)	0.83 (1)	6.16% (1)	1.0 (1)
GPM_EARLY*	0.63 (4)	0.61 (6)	25.92% (7)	5.7 (6)
GPM_LATE*	0.62 (5)	0.57 (8)	24.53% (6)	6.3 (7)
PERSIANN*	0.45 (9)	0.59 (7)	26.49% (8)	8.0 (8)
PERSIANN_CCS*	0.29 (10)	0.36 (10)	39.70% (10)	10.0 (10)
Satellite-gauge precipitation (SG) product				
CMORPH_BLD	0.53 (7)	0.71 (5)	12.25% (3)	5.0 (4)
CHIRPS	0.70 (2)	0.74 (3)	15.69% (4)	3.0 (3)
GPM_FINAL	0.62 (6)	0.72 (4)	18.06% (5)	5.0 (4)
PERSIANN_CDR	0.49 (8)	0.56 (9)	31.63% (9)	8.7 (9)
Ensemble products				
MSWEP	0.69 (3)	0.80 (2)	6.34% (2)	2.33 (2)

Figure 4. Scatter plots comparing average annual rainfall (2001-2021) from GGR and ten SPE products across 98 sub-catchments

Table 6. Statistical metrics at station E.20A during calibration and validation period using GGR and ten SPE products

GGR and SPE		Calibration (2001-2015)					Validation (2016-2021)				
		NSE	KGE_E	KGE_L	KGE_F	AVG	NSE	KGE_E	KGE_L	KGE_F	AVG
	GGR	**0.69**	**0.80**	**0.56**	**0.85**	**0.73**	**0.83**	**0.69**	**0.43**	**0.69**	**0.66**
S	CHRIP*	0.66	0.79	0.54	0.85	**0.71**	0.72	0.80	0.45	0.85	**0.71**
S	GPM_EARLY*	0.75	0.82	0.53	0.86	**0.74**	0.71	0.54	0.39	0.55	**0.55**
S	GPM_LATE*	0.63	0.63	0.57	0.65	**0.62**	0.79	0.75	0.45	0.77	**0.69**
S	PERSIANN*	0.46	0.62	0.52	0.67	**0.57**	0.66	0.79	0.38	0.89	**0.68**
S	PERSIANN_CCS*	-0.06	0.46	0.52	0.56	**0.37**	-0.38	-0.17	0.43	-0.16	**-0.07**
SG	CMORPH_BLD	0.71	0.85	0.53	0.93	**0.76**	0.48	0.35	0.48	0.35	**0.41**
SG	CHRIPS	0.71	0.83	0.54	0.89	**0.74**	0.76	0.79	0.46	0.81	**0.70**
SG	GPM_FINAL	0.78	0.82	0.54	0.84	**0.75**	0.79	0.74	0.48	0.75	**0.69**
SG	PERSIANN_CDR	0.57	0.71	0.55	0.76	**0.65**	0.61	0.73	0.48	0.77	**0.65**
EN	MSWEP	0.78	0.89	0.53	0.95	**0.79**	0.86	0.92	0.49	0.96	**0.81**
AVG S		0.49	0.67	0.54	0.72	**0.60**	0.50	0.54	0.42	0.58	**0.51**
AVG SG		0.69	0.80	0.54	0.85	**0.72**	0.66	0.65	0.47	0.67	**0.61**

Note: * indicates S products

Table 7. Average statistical metrics across eight stations during calibration and validation period using GGR and ten SPE products

GGR and SPE		Calibration (2001-2015)					Validation (2016-2021)				
		NSE	KGE_E	KGE_L	KGE_F	AVG	NSE	KGE_E	KGE_L	KGE_F	AVG
	GGR	**0.78**	**0.83**	**0.63**	**0.86**	**0.77**	**0.78**	**0.74**	**0.63**	**0.76**	**0.72**
S	CHRIP*	0.63	0.78	0.64	0.88	**0.73**	0.13	0.42	0.60	0.47	**0.40**
S	GPM_EARLY*	0.69	0.70	0.57	0.75	**0.68**	0.61	0.41	0.55	0.42	**0.50**
S	GPM_LATE*	0.66	0.71	0.62	0.76	**0.69**	0.54	0.41	0.60	0.45	**0.50**
S	PERSIANN*	0.37	0.56	0.52	0.69	**0.54**	0.63	0.80	0.52	0.89	**0.71**
S	PERSIANN_CCS*	-0.05	0.46	0.57	0.68	**0.42**	-1.31	-0.57	0.50	-0.56	**-0.49**
SG	CMORPH_BLD	0.68	0.82	0.64	0.90	**0.76**	0.47	0.46	0.61	0.48	**0.50**
SG	CHRIPS	0.74	0.83	0.64	0.89	**0.78**	0.68	0.74	0.63	0.76	**0.70**
SG	GPM_FINAL	0.80	0.84	0.63	0.87	**0.78**	0.73	0.68	0.61	0.70	**0.68**
SG	PERSIANN_CDR	0.59	0.71	0.65	0.78	**0.69**	0.34	0.49	0.64	0.51	**0.49**
EN	MSWEP	0.77	0.84	0.66	0.89	**0.79**	0.82	0.84	0.68	0.86	**0.80**
AVG S		0.46	0.64	0.58	0.75	**0.61**	0.12	0.30	0.55	0.33	**0.33**
AVG SG		0.70	0.80	0.64	0.86	**0.75**	0.55	0.59	0.62	0.61	**0.59**

Note: * indicates S products

5. CONCLUSIONS

This study assessed the performance of ten Satellite-based Precipitation Estimate (SPE), grouped into satellite-based, satellite-gauge combined, and ensemble categories, for runoff estimation using the FLEX-TOPO-SD hydrological model in the CRB. Runoff outputs generated from each SPE product were compared against those obtained using gridded gauged rainfall (GGR) data at eight stations. The goal was to evaluate how reliably each SPE product could serve as an alternative input for hydrological modelling in regions with limited ground-based data.

The accuracy of ten Satellite-based Precipitation Estimate (SPE) products was assessed against gridded gauged rainfall (GGR) data in the CRB over the period 2001–2021. Overall, satellite-gauge (SG) products showed better agreement with GGR than satellite-only (S) products. Nevertheless, CHIRP*—an S product—also demonstrated strong performance. Across daily, monthly, and annual timescales, MSWEP, GPM_FINAL, CMORPH_BLD, CHIRPS, and CHIRP* consistently provided the most accurate rainfall estimates. Statistical analysis and scatter plot comparisons of average annual rainfall across 98 sub-catchments identified CHIRP*, MSWEP, and CHIRPS as the top-performing products overall, while the PERSIANN family consistently exhibited the poorest performance.

Runoff estimation was conducted using the FLEX-TOPO-SD model with GGR and the ten SPE products at station E.20A and across eight additional stations. During calibration, MSWEP and GPM_FINAL achieved the highest NSE value (0.78), while in validation, MSWEP maintained the highest performance (NSE = 0.86), followed by GGR (0.83) and GPM_FINAL (0.79).

Across all eight stations, GPM_FINAL performed best during calibration (NSE = 0.80), followed by GGR (0.78), MSWEP (0.77), and CHIRPS (0.74). In validation, MSWEP led (NSE = 0.82), followed by GGR (0.78), GPM_FINAL (0.73), and CHIRPS (0.68). SG products consistently outperformed S products, as indicated by higher average NSE values. The PERSIANN family, particularly PERSIANN_CCS*, exhibited the weakest performance, with negative NSE values in both calibration and validation.

These findings highlight the strong potential of specific SPE products—particularly MSWEP, GPM_FINAL, and CHIRPS—as reliable alternatives to gauge-based rainfall data (such as GGR) for hydrological modeling in data-scarce regions. The results also confirm the effectiveness and applicability of the FLEX-TOPO-SD model for runoff estimation across multiple sub-catchments in regional hydrological studies.

REFERENCES

Arnold, J. G., Moriasi, D. N., Gassman, P. W., Abbaspour, K. C., White, M. J., Srinivasan, R., Santhi, C., Harmel, R., Van Griensven, A., & Van Liew, M. W. (2012). SWAT: Model use, calibration, and validation. Transactions of the ASABE, 55(4), 1491-1508.

Beck, H. E., Van Dijk, A. I., Levizzani, V., Schellekens, J., Miralles, D. G., Martens, B., & De Roo, A. (2017). MSWEP: 3-hourly 0.25 global gridded precipitation (1979–2015) by merging gauge, satellite, and reanalysis data. Hydrology and Earth System Sciences, 21(1), 589-615.

Beck, H. E., Wood, E. F., Pan, M., Fisher, C. K., Miralles, D. G., Van Dijk, A. I., McVicar, T. R., & Adler, R. F. (2019). MSWEP V2 global 3-hourly 0.1 precipitation: methodology and quantitative assessment. Bulletin of the American Meteorological Society, 100(3), 473-500.

Dao, V., Arellano, C. J., Nguyen, P., Almutlaq, F., Hsu, K., & Sorooshian, S. (2025). Bias correction of satellite precipitation estimation using Deep Neural Networks and topographic information over the Western US. Journal of Geophysical Research: Atmospheres, 130(4), e2024JD042181.

Fenicia, F., Savenije, H. H., Matgen, P., & Pfister, L. (2008). Understanding catchment behavior through stepwise model concept improvement. Water Resources Research, 44(1).

Funk, C., Peterson, P., Landsfeld, M., Pedreros, D., Verdin, J., Shukla, S., Husak, G., Rowland, J., Harrison, L., & Hoell, A. (2015). The climate hazards infrared precipitation with stations—a new environmental record for monitoring extremes. Scientific data, 2(1), 1-21.

Gan, T. Y., Dlamini, E. M., & Biftu, G. F. (1997). Effects of model complexity and structure, data quality, and objective functions on hydrologic modeling. Journal of Hydrology, 192(1-4), 81-103.

Gao, H., Hrachowitz, M., Fenicia, F., Gharari, S., & Savenije, H. (2014). Testing the realism of a topography-driven model (FLEX-Topo) in the nested catchments of the Upper Heihe, China. Hydrology and Earth System Sciences, 18(5), 1895-1915.

Gao, H., Hrachowitz, M., Sriwongsitanon, N., Fenicia, F., Gharari, S., & Savenije, H. H. (2016). Accounting for the influence of vegetation and landscape improves model transferability in a tropical savannah region. Water Resources Research, 52(10), 7999-8022.

Gassman, P. W., Sadeghi, A. M., & Srinivasan, R. (2014). Applications of the SWAT model special section: overview and insights. Journal of Environmental Quality, 43(1), 1-8.

Gautam, J., O, S., Vinod, D., & Mahesha, A. (2024). Evaluation of GPM IMERG satellite precipitation for rainfall–runoff modelling in Great Britain. Hydrological Sciences Journal, 69(14), 2010-2025.

Ghosh, A., Roy, M. B., & Roy, P. K. (2022). Evaluating the performance of MIKE NAM model on rainfall–runoff in lower Gangetic floodplain, West Bengal, India. Modeling Earth Systems and Environment, 8(3), 4001-4017.

Gumindoga, W., Rientjes, T.H.M., Haile, A.T., Makurira, H., Reggiani, P., 2019. Performance of bias-correction schemes for CMORPH rainfall estimates in the Zambezi

Habib, E., Haile, A. T., Sazib, N., Zhang, Y., & Rientjes, T. (2014). Effect of bias correction of satellite-rainfall estimates on runoff simulations at the source of the Upper Blue Nile. Remote Sensing, 6(7), 6688-6708.

Hlaing, P. T., Humphries, U. W., & Waqas, M. (2024). Hydrological model parameter regionalization: Runoff estimation using machine learning techniques in the Tha Chin River Basin, Thailand. MethodsX, 13, 102792.

Hsu, K.-l., Gao, X., Sorooshian, S., & Gupta, H. V. (1997). Precipitation estimation from remotely sensed information using artificial neural networks. Journal of applied meteorology, 36(9), 1176-1190.

Hughes, D. A. (2006). Comparison of satellite rainfall data with observations from gauging station networks. Journal of Hydrology, 327(3-4), 399-410.

Huffman, G. J., Adler, R. F., Bolvin, D. T., & Nelkin, E. J. (2010). The TRMM multi-satellite precipitation analysis (TMPA). Satellite rainfall applications for surface hydrology, 3-22.

Huffman, G. J., Bolvin, D. T., Nelkin, E. J., Wolff, D. B., Adler, R. F., Gu, G., Hong, Y., Bowman, K. P., & Stocker, E. F. (2007). The TRMM multisatellite precipitation analysis (TMPA): Quasi-global, multiyear, combined-sensor precipitation estimates at fine scales. Journal of Hydrometeorology, 8(1), 38-55.

Hussein, K., Alhosani, N., Al-Areeq, A. M., Al Aghbari, A. A., Elkamali, M., Alsumaiti, T., Sharif, H. O., Almurshidi, A. M., & Abdalati, W. (2025). Unprecedented rainfall in the United Arab Emirates: hydrologic and flood impact analysis of the April 2024 event. Natural Hazards, 1-23.

Jahanshahi, A., Roshun, S. H., & Booij, M. J. (2024). Comparison of satellite-based and reanalysis precipitation products for hydrological modeling over a data-scarce region. Climate Dynamics, 62(5), 3505-3537.

Joyce, R. J., Janowiak, J. E., Arkin, P. A., & Xie, P. (2004). CMORPH: A method that produces global precipitation estimates from passive microwave and infrared data at high spatial and temporal resolution. Journal of Hydrometeorology, 5(3), 487-503.

Kaprom, C., Williams, J. A., Mehrotra, R., Ophaphaibun, C., & Sriwongsitanon, N. (2025). A comprehensive evaluation of the accuracy of satellite-based precipitation estimates over Thailand. Journal of Hydrology: Regional Studies, 59, 102380.

Kidd, C., Huffman, G., 2011. Global precipitation measurement. Meteorol. Appli 18 (3), 334–353. https://doi.org/10.1002/met.284.

Liu, Y., Wei, Z., Yang, B., & Cui, Y. (2025). An unsupervised adaptive fusion framework for satellite-based precipitation estimation without gauge observations. Journal of Hydrology, 646, 132341.

Malone, T. (1999). Using URBS for real time flood modelling. Water 99: Joint Congress; 25th Hydrology & Water Resources Symposium, 2nd International Conference on Water Resources & Environment Research; Handbook and Proceedings,

Mapiam, P. P., & Sriwongsitanon, N. (2009). Estimation of the URBS model parameters for flood estimation of ungauged catchments in the upper Ping river basin, Thailand. ScienceAsia, 35(2009), 49-56.

Miralles, D. G., Bonte, O., Koppa, A., Baez-Villanueva, O. M., Tronquo, E., Zhong, F., ... & Haghdoost, S. (2025). GLEAM4: global land evaporation and soil moisture dataset at 0.1 resolution from 1980 to near present. Scientific Data, 12(1), 416.

Muñoz, P., Muñoz, D. F., Orellana-Alvear, J., & Célleri, R. (2025). Enhancing runoff forecasting through the integration of satellite precipitation data and hydrological knowledge into machine learning models. Natural Hazards, 121(4), 3915-3937.

Nadeem, M.U., Waheed, Z., Ghaffar, A.M., Javaid, M.M., Hamza, A., Ayub, Z., Nawaz, M.A., Waseem, W., Hameed, M.F., Zeeshan, A., 2022. Application of HEC-HMS for flood forecasting in hazara catchment Pakistan, south Asia. Int. J. Hydrol. 6 (1), 7–12. https://doi.org/10.15406/ijh.2022.06.00296.

Nguyen, B.Q., Van Binh, D., Tran, T.N.D., Kantoush, S.A., Sumi, T., 2024. Response of streamflow and sediment variability to cascade dam development and climate change in the Sai Gon Dong Nai River basin. Clim. Dyn. 62 (8), 7997–8017. https://doi.org/10.1007/s00382-024-07319-7.

Nguyen, V. D., Rouzegari, N., Dao, V., Almutlaq, F., Nguyen, P., & Sorooshian, S. (2025). Comparative Analysis of Satellite-Based Precipitation Products During Extreme Rainfall from Super Typhoon Yagi in Hanoi, Vietnam (September 2024). Remote Sensing, 17(9), 1598.

Ponomarjovs, P., Draesner, F., & Fuchs, S. (2025). A general methodological framework for hazard assessment in remote mountain areas combining geomorphological mapping with UAV survey. Journal of Mountain Science, 22(3), 763-775.

Prasertthonggorn, N., & Sriwongsitanon, N. (2022). Performance Comparison of Remotely Sensed ET Products using KU-FLEX-TOPO-SD and Water Balance for Chi River Basin (Master's thesis, Kasetsart University).

Quan, Q., Liang, W., Yan, D., & Lei, J. (2022). Influences of joint action of natural and social factors on atmospheric process of hydrological cycle in Inner Mongolia, China. Urban climate, 41, 101043.

Ranjan, N., Tamboli, M., Prasad, J. R., Prasad, R. S., & Dhumane, A. V. (2025). Deep learning-driven rainfall prediction leveraging hybrid child drawing development optimization and time series data. Earth Science Informatics, 18(3), 280.

Savenije, H. H. (2010). HESS Opinions" Topography driven conceptual modelling (FLEX-Topo)". Hydrology and Earth System Sciences, 14(12), 2681-2692.

Sharma, K., & Singh, S. (1992). Runoff estimation using Landsat Thematic Mapper data and the SCS model. Hydrological sciences journal, 37(1), 39-52.

Skofronick-Jackson, G., Petersen, W.A., Berg, W., Kidd, C., Stocker, E.F., Kirschbaum, D.B., Kakar, R., Braun, S.A., Huffman, G.J., Iguchi, T., Kirstetter, P.E., 2017. The Global Precipitation Measurement (GPM) mission for science and society. Bull. Am. Meteorol. Soc. 98 (8), 1679–1695. https://doi.org/10.1175/BAMS-D-15-00306.1.

Sorooshian, S., Hsu, K.-L., Gao, X., Gupta, H. V., Imam, B., & Braithwaite, D. (2000). Evaluation of PERSIANN system satellite-based estimates of tropical rainfall. Bulletin of the American Meteorological Society, 81(9), 2035-2046.

Sriwongsitanon, N. (2010). Flood forecasting system development for the Upper Ping River Basin. Agriculture and Natural Resources, 44(4), 717-731.

Sriwongsitanon, N., Gao, H., Savenije, H. H., Maekan, E., Saengsawang, S., & Thianpopirug, S. (2016). Comparing the Normalized Difference Infrared Index (NDII) with root zone storage in a lumped conceptual model. Hydrology and Earth System Sciences, 20(8), 3361-3377.

Sriwongsitanon, N., Jandang, W., Williams, J., Suwawong, T., Maekan, E., & Savenije, H. H. (2023). Using normalised difference infrared index patterns to constrain semi-distributed rainfall–runoff models in tropical nested catchments. Hydrology and Earth System Sciences, 27(11), 2149-2171.

Sriwongsitanon, N., Kaprom, C., Tantisuvanichkul, K., Prasertthonggorn, N., Suiadee, W., Bastiaanssen, W. G., & Williams, J. A. (2023). The Combined Power of Double Mass Curves and Bias Correction for the Maximisation of the Accuracy of an Ensemble Satellite-Based Precipitation Estimate Product. *Hydrology*, *10*(7), 154.

Tapas, M.R., Do, S.K., Etheridge, R., Lakshmi, V., 2024. Investigating the impacts of climate change on hydroclimatic extremes in the Tar-Pamlico River basin, North Carolina. J. Environ. Manag. 363, 121375. https://doi.org/10.1016/j.jenvman.2024.121375.

Wen, Y., Schuur, T., Vergara, H., Kuster, C., 2021. Effect of precipitation sampling error on flash flood monitoring and prediction: Anticipating operational rapidupdate polarimetric weather radars. J. Hydrometeorol. 22 (7), 1913–1929. https://doi.org/10.1175/JHM-D-19-0286.1.

Zamani, A. S., Dabove, P., Bagheri, M., & Naboureh, A. (2025). Thesis Subject: Examining the impact of climate change in the Apennine Mountains: A Remote Sensing-based Data Analysis.

Zhou, L., Koike, T., Takeuchi, K., Rasmy, M., Onuma, K., Ito, H., Selvarajah, H., Liu, L., Li, X., & Ao, T. (2022). A study on availability of ground observations and its impacts on bias correction of satellite precipitation products and hydrologic simulation efficiency. Journal of Hydrology, 610, 127595.